Direct evidence for mode-specific vibrational energy relaxation from quantum time-dependent perturbation theory. III. The ν_4 and ν_7 modes of nonplanar nickel porphyrin models

Yong Zhang[a] and John E. Straub[b]
Department of Chemistry, Boston University, Boston, Massachusetts 02215, USA

(Received 11 February 2009; accepted 12 May 2009; published online 4 June 2009)

The time scales and pathways of vibrational energy relaxation (VER) of the ν_4 and ν_7 modes of three nickel porphyrin models, nickel porphine (NiP), nickel protoporphyrin IX (Ni-heme), and nickel octaethylporphyrin (NiOEP), were studied using a non-Markovian time-dependent perturbation theory at the B3LYP/6-31G(d) level. When NiP is calculated with D_{4h} symmetry, it has the planar structure and the same VER properties as ferrous iron porphine (FeP). The porphine cores of both Ni-heme and NiOEP were distorted from a planar geometry, assuming a nonplanar structure, similar to that of the heme structure in cytochrome c. The VER time scales of Ni-heme are found to be similar to those predicted for a planar iron heme, but the derived pathways have distinctly different features. In particular, the strong coupling between the ν_7 mode and the overtone of the $\sim 350\ \mathrm{cm}^{-1}$ γ_7 mode, observed for planar porphyrins, is absent in both nonplanar nickel porphyrins. Direct energy exchange between the ν_4 and ν_7 modes is not observed in NiOEP, but is found to play an essential role in the VER of the ν_4 mode in Ni-heme. The Ni-heme isopropionate groups are involved in the dominant VER pathways of both the ν_4 and ν_7 modes of Ni-heme. However, in contrast with VER pathways derived in planar iron heme, the isopropionate groups are not observed to play an essential role relative to other side chains in spatially directing the vibrational energy flow. © *2009 American Institute of Physics*. [DOI: 10.1063/1.3147704]

I. INTRODUCTION

Myoglobin (Mb) and cytochrome c (Cyt c) are heme proteins in which axial ligands coordinating the central heme Fe atom can be dissociated by photoexcitation. This process is accompanied by vibrational excitation of the axial ligand, heme, and surrounding protein residues.[1–3] Distinct features of the evolution of vibrational energy transfer following photodissociation have been observed in both experimental and computational studies on these two heme proteins.[4–10] Those studies predicted detailed insight into the nature of ultrafast energy transfer and conformational change and raised many questions related to fundamental aspects of the energy transfer process. An outstanding challenge to theoretical biophysics is the development of theoretical methods that provide an accurate description of these fundamental energy transfer processes.

The crystal structures of Mb[11,12] and Cyt c (Ref. 13) indicate that the heme moiety assures significantly different configurations in each protein. As shown in Fig. 1 (top panel), most atoms of the porphine core of the Mb heme remain in a plane with the exception of two carbon atoms in the *A* and *C* pyrrole rings. In Cyt c the heme is distorted by the contacts with the surrounding protein residues. The distinct heme geometries result in distinct time scales and mechanisms for heme cooling in Mb and Cyt c.[14] Using molecular dynamics simulations, the solvent dependence of the time scales and pathways of heme cooling in both Mb and Cyt c following photoexcitation have been studied.[14,15] A dramatic solvent dependence was observed for Mb but no solvent dependence was found for Cyt c. These distinctly different energy transfer processes can be intimately related to aspects of the heme protein geometry that support protein function.

Coherence spectroscopy has been applied to study the heme excitation properties following ligand dissociation in Mb and Cyt c.[16–21] Using a sub-10-fs pulse, the mode-specific response of the heme following photoexcitation was studied by Miller and co-workers.[22] It was found that the heme ν_7 mode was highly excited following photodissociation of CO in MbCO. No similar signal was observed for Cyt c following the photodissociation of the Met80 ligand.

Using time-resolved resonance Raman (TR^3) spectroscopy, Kitagawa and co-workers monitored the intriguing mode-specific behavior of heme vibrational relaxation following ligand dissociation.[23–26] For Mb, it was found that the ν_4 and ν_7 modes were highly excited during the reaction and the decay time constants were found to be 1.1 ± 0.6 ps for the ν_4 band and 1.9 ± 0.6 ps for the ν_7 band, implying a thermal decay of the heme within 2 ps.[25,26] As a model of the heme moiety, metalloporphyrins have been studied[27–29] and similar mode-specific properties were observed.[30–32] For nickel octaethylporphyrin (NiOEP) in various organic solvents, the anti-Stokes band of the ν_4 mode rose immediately following photoexcitation, whereas the ν_7 band had a delay

[a]Present address: Chemistry Department, University of Utah, 315 S. 1400 E., Salt Lake City, UT 84112. Electronic mail: zhangy@hec.utah.edu.
[b]Author to whom correspondence should be addressed. Electronic mail: straub@bu.edu.

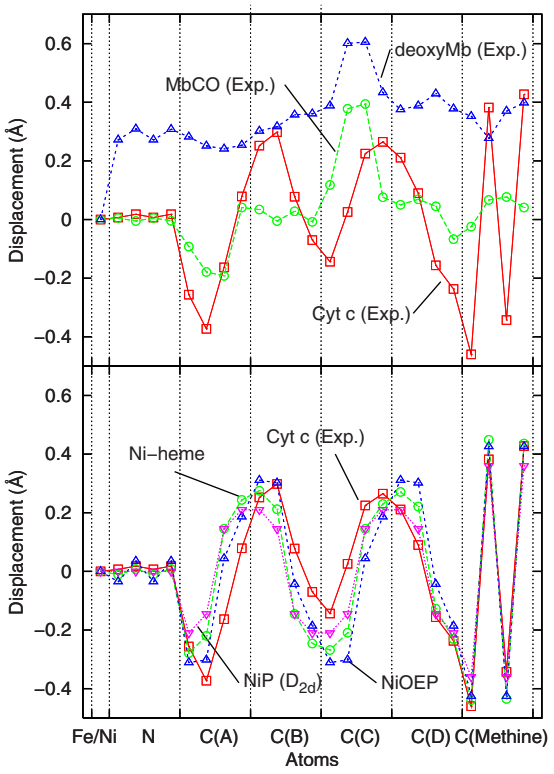

FIG. 1. (Color online) The displacements of the porphine core atoms relative to the porphyrin plane defined by the four pyrrole nitrogen atoms (with origin centered at the Fe or Ni atom). The x axis is in the order of iron/nickel, pyrrole nitrogens, pyrrole carbons (rings A, B, C, and D as shown in Fig. 2), and methine carbons. Top panel: The displacements derived from Cyt c [protein data bank (PDB) entry 1HRC (Ref. 13)], MbCO [PDB entry 1MBC (Ref. 11)] and deoxyMb [PDB entry 1BZP (Ref. 12)] crystal structures. Bottom panel: The displacements derived from the optimized NiP (with D_{2d} symmetry), Ni-heme, and NiOEP structure computed at the B3LYP/6-31G(d) level. Values derived from the Cyt c crystal structure are plotted for reference.

of ~2.5 ps. Both modes relaxed with time constants around 10 ps, significantly slower than those observed for heme relaxation in Mb.[30]

In previous work,[33,34] we explored mode-specific vibrational energy transfer in several iron porphyrin models with triplet or quintuplet spin states. Those models were chosen to mimic the heme in the active site of Mb. Using non-Markovian time-dependent perturbation theory informed by DFT calculations, we observed that the in-plane ν_7 mode strongly couples to the overtone of the methine wagging motion γ_7. We also found that the two heme isopropionate groups play an essential role in the important energy relaxation pathways responsible for heme cooling, consistent with previous computational[8,9,15] and experimental[35–37] observations. No direct energy transfer was found between the ν_4 mode and the ν_7 mode for any of the iron porphyrins studied.

In this work, we explore the mode-specific VER properties of three nickel porphyrin models, nickel porphine (NiP), nickel protoporphyrin IX (Ni-heme), and NiOEP at the B3LYP/6-31G(d) level. The porphine cores of Ni-heme and NiOEP are distorted from a planar structure, with the degree of nonplanar distortion being similar to that observed for the heme in Cyt c. We find that the vibrational energy relaxation (VER) properties of the pure planar NiP (with D_{4h} symmetry) are similar to FeP, independent of the central metal. In Ni-heme and NiOEP, the coupling between the ν_7 mode and the overtone of the γ_7 mode is weaker than in NiP (D_{4h}) and iron porphyrins. While in NiOEP, no coupling between the ν_4 and ν_7 modes is observed, the ν_7 mode is found to play an important role in VER of the ν_4 mode in Ni-heme.

II. THEORY AND METHODS

A. Time-dependent perturbation theory

The VER theory[38] employed in this work is briefly summarized. We expand the potential energy surface with respect to the normal coordinates of the system, q_S, and bath, q_α, and their frequencies, ω_S and ω_α, up to third and fourth order nonlinear couplings,

$$H = H_S + H_B - q_S \delta F + q_S^2 \delta G, \tag{1}$$

$$H_S = \frac{p_S^2}{2} + V(q_S), \tag{2}$$

$$H_B = \sum \left(\frac{p_\alpha^2}{2} + \frac{\omega_\alpha^2 q_\alpha^2}{2} \right), \tag{3}$$

$$\delta F = \sum_{\alpha,\beta} C_{S\alpha\beta} (q_\alpha q_\beta - \langle q_\alpha q_\beta \rangle), \tag{4}$$

$$\delta G = \sum_{\alpha,\beta} C_{SS\alpha\beta} (q_\alpha q_\beta - \langle q_\alpha q_\beta \rangle) + \sum_\alpha C_{SS\alpha} q_\alpha, \tag{5}$$

where H_S (H_B) is the system (bath) Hamiltonian and $C_{S\alpha\beta}$ ($C_{SS\alpha\beta}$) are the third (fourth) order coupling terms. From the von Neumann–Liouville equation, a reduced density matrix for the system mode is derived using the time-dependent perturbation theory after tracing over the bath degrees of freedom. The commonly employed Markov approximation, which assumes a separation in time scale between the relaxation of the system and bath modes, is not invoked in this theory. The final VER formula is

$$\begin{aligned}(\rho_S)_{00}(t) \simeq & \frac{2}{\hbar^2} \sum_{\alpha,\beta} [C_{--}^{\alpha\beta} u_t(\tilde{\omega}_S - \omega_\alpha - \omega_\beta) \\ & + C_{++}^{\alpha\beta} u_t(\tilde{\omega}_S + \omega_\alpha + \omega_\beta) + C_{+-}^{\alpha\beta} u_t(\tilde{\omega}_S - \omega_\alpha + \omega_\beta)] \\ & + \frac{2}{\hbar^2} \sum_\alpha [C_-^\alpha u_t(\tilde{\omega}_S - \omega_\alpha) + C_+^\alpha u_t(\tilde{\omega}_S + \omega_\alpha)],\end{aligned} \tag{6}$$

where the subscript of $(\rho_S)_{00}$ indicates the vibrational ground state and $u_t(\Omega)$ is defined as

$$u_t(\Omega) = \int_0^t dt' \int_0^{t'} dt'' \cos \Omega(t' - t'') = \frac{1 - \cos \Omega t}{\Omega^2}. \tag{7}$$

The coefficients, $C_{--}^{\alpha\beta}$, $C_{++}^{\alpha\beta}$, $C_{+-}^{\alpha\beta}$, C_-^α, and C_+^α, can be derived from the nonlinear coupling constants $C_{S\alpha\beta}$ and $C_{SS\alpha\beta}$.[38] When the system mode is excited to the $\nu=1$ state, VER is described by the decay of the reduced density matrix element most simply as $\rho_{11}(t) = 1 - \rho_{00}(t) \simeq \exp[-\rho_{00}(t)]$ under the cumulant approximation.

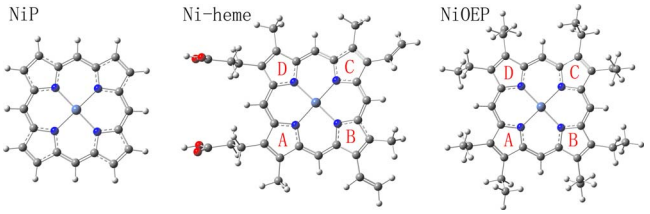

FIG. 2. (Color online) Depiction of the optimized structure of the NiP, Ni-heme, and NiOEP at the B3LYP/6-31G(d) level. The four pyrrole rings, A, B, C, and D, are labeled for Ni-heme and NiOEP. The core sizes, the average distance between Ni and pyrrole N atoms, were found to be 1.957, 1.939, and 1.940 Å for NiP (D_{4h}), Ni-heme, and NiOEP, respectively.

B. Simulation procedure

Three four-coordinate nickel porphyrin models, the NiP, a porphyrin model without side chains, the Ni-heme, a nickel substituted heme, and the NiOEP, were studied in this work. The three nickel porphyrin models were optimized to their singlet ground states.[39] Normal mode analysis was carried out for each optimized structure. The "verytight" self-consistent field convergence criterion and "ultrafine" integration grid were applied. The third and fourth order anharmonic coupling constants were calculated using a numerical finite-difference method.[40] All calculations were performed using the GAUSSIAN03 package[41] at the B3LYP/6-31G(d) level.

The system mode VER rate constant was derived by fitting the reduced density matrix element $\rho_{11}(t)$ time profile. The energy transfer pathways were identified by calculating the third order Fermi resonance parameters defined as

$$r_{S\alpha\beta} = \frac{|C_{S\alpha\beta}|}{\hbar|\tilde{\omega}_S - \omega_\alpha - \omega_\beta|}\sqrt{\frac{\hbar}{2\tilde{\omega}_S}}\sqrt{\frac{\hbar}{2\omega_\alpha}}\sqrt{\frac{\hbar}{2\omega_\beta}}, \tag{8}$$

where $\tilde{\omega}_S$ and ω_α are the frequencies of system mode and bath mode, respectively.

The geometrical overlap of the system mode, S, and bath modes, α and β, was calculated following Kidera's definition,[42]

$$G_3(S,\alpha,\beta) = \sum_{i=1}^{N_{\text{atom}}} m_i^{3/2}|\mathbf{v}_{iS}||\mathbf{v}_{i\alpha}||\mathbf{v}_{i\beta}|, \tag{9}$$

where N_{atom} is the number of atoms in the molecule, m_i is the mass of atom i, and $\mathbf{v}_{i\alpha}$ is the calculated eigenvector for mode α and atom i. Large values of G_3 imply strong spatial overlap of the system and specified bath modes.

III. RESULTS AND DISCUSSIONS

The optimized structure of the three nickel porphyrin models, NiP, nickel substituted protoporphyrin IX (Ni-heme), and NiOEP, are depicted in Fig. 2. NiP was calculated in both D_{4h} and D_{2d} symmetries with NiP (D_{2d}) being the global minimum. NiP (D_{4h}) is found to be planar, whereas the porphine core in NiP (D_{2d}), Ni-heme, and NiOEP is found to be displaced from the plane defined by the four pyrrole nitrogen atoms. This results from the drive to lower the energy by shortening bond lengths (with the expense of decreased electronic overlap).[43] The displacement of each atom from the plane defined by the pyrrole nitrogens is shown in Fig. 1 (bottom panel). The atom displacements derived from the Cyt c crystal structure[13] are also depicted. The calculated porphine core structures of Ni-heme and NiOEP qualitatively agree with the core structure of the heme in Cyt c.

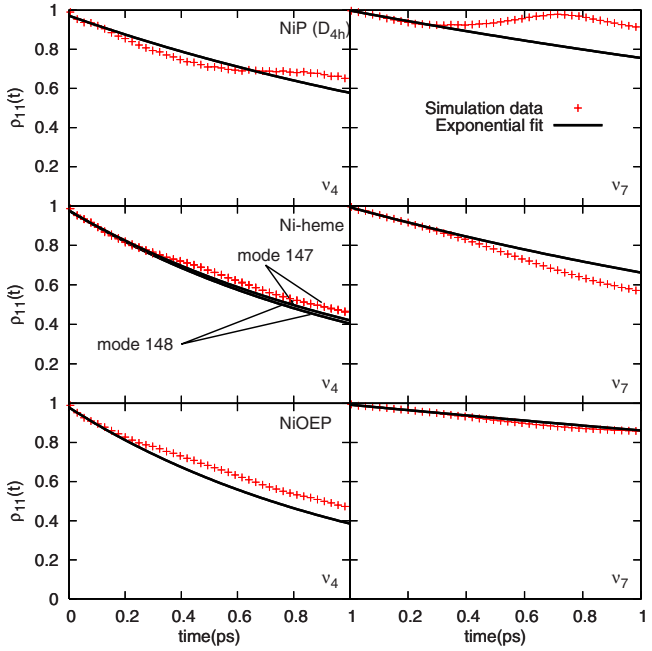

FIG. 3. (Color online) The time evolution of the initially excited density matrix element ρ_{11} for the ν_4 and ν_7 modes of NiP (with D_{4h} symmetry, top), Ni-heme (middle), and NiOEP (bottom). The simulation data are shown as points and the single-exponential fit to the initial decay is shown as a solid line. The fitted time constants are summarized in Table I.

Normal modes were calculated for the optimized nickel porphyrin models. The time scales of VER of the excited ν_4 and ν_7 modes were derived using the time-dependent perturbation theory and the pathways were identified by calculating the third order Fermi resonance parameters.

A. VER of NiP modes

NiP has been reported to be the only planar nickel porphyrin model.[44] In this work, a planar structure with D_{4h} symmetry was obtained and the core size was found to be 1.957 Å. This core is smaller than that of FeP (1.988 Å) (Ref. 34) due to the smaller size of the Ni atom relative to the Fe atom. Normal mode analysis reveals that this structure has one imaginary frequency, which is associated with ruffling motion and a frequency of -26.9 cm^{-1}, consistent with previous calculations by Spiro and co-workers.[45] This low frequency imaginary mode was ignored when applying the time-dependent perturbation theory. Ignoring this imaginary mode does not affect the final results or conclusions.[38] The ν_4, ν_7, and γ_7 modes were identified as modes 78, 34, and 15, respectively. The ν_4 and ν_7 modes were treated independently as the system mode and the reduced density matrix elements were fitted using a single exponential decay function as shown in Fig. 3 (top). The relaxation time constants are summarized in Table I. The calculated third order Fermi resonance parameter $r_{S\alpha\beta}$ of the important VER pathways

TABLE I. Summary of system mode frequencies (harmonic and anharmonic), mode assignments, and VER time constants studied for NiP (with D_{4h} and D_{2d} symmetries, respectively), Ni-heme, and NiOEP.

Mode number	Frequency (cm^{-1})		T_1 (ps)		Assignment
	Harm (ω_S)	Anharm ($\tilde{\omega}_S$)	Simulation	Experiment	
			NiP (D_{4h}, planar)		
78	1417.0	1414.0	1.9 ± 0.2		ν_4
34	745.0	743.0	3.6 ± 0.1		ν_7
15	348.0	347.7	42.3 ± 25.3		γ_7
			NiP (D_{2d}, nonplanar)		
78	1417.2	1413.7	1.8 ± 0.2		ν_4
34	745.4	742.4	3.4 ± 0.2		ν_7
15	349.1	353.1	24.1 ± 8.9		γ_7
			Ni-heme		
148	1421.1	1418.7	1.1 ± 0.0	1.1 ± 0.6[a]	ν_4
147	1419.9	1418.8	1.2 ± 0.1	1.1 ± 0.6	ν_4
74	699.7	703.1	2.5 ± 0.1	1.9 ± 0.6	ν_7
47	348.4	357.6	5.4 ± 0.2		γ_7
			NiOEP		
157	1422.5	1421.2	1.1 ± 0.0	11 ± 2[b]	ν_4
74	715.5	718.0	7.0 ± 0.4	10 ± 2	ν_7
51	348.6	359.6	13.0 ± 2.4		γ_7

[a]Data for carboxy Mb (Ref. 24).
[b]Data for NiOEP in benzene (Ref. 30).

($r_{S\alpha\beta} \geq 0.05$) as well as the important coupling constants $C_{S\alpha\beta}$ and the frequency resonance parameter $1/|\tilde{\omega}_S - \omega_\alpha - \omega_\beta|$ are plotted in Fig. 4.

For both ν_4 and ν_7, the frequencies in NiP (D_{4h}) are a little higher than in FeP (by ~14 and ~5 cm^{-1}, respectively) as a result of the structural difference. However, the VER time constants (1.9 ± 0.2 ps for ν_4 and 3.6 ± 0.1 ps for ν_7) are almost the same as FeP (2.1 ± 0.2 ps for ν_4 and 3.6 ± 0.4 ps for ν_7).[34] No obvious difference in the energy transfer pathways was observed. For the six important energy transfer pathways from the excited ν_4 mode, four (30+30, 31+31, 32+32, and 33+33) are formed by porphyrin out-of-plane modes and two (54+17 and 55+18) are formed by porphyrin in-plane motions. No mixed porphyrin out-of-plane/in-plane pathway was found. For the excited ν_7 mode, the dominant energy transfer pathway is defined by the strong coupling to the overtone of mode 15, the Ni out-of-plane γ_7 mode, reflected in a large Fermi resonance parameter ($r_{S\alpha\beta}$=0.091). Whereas the alternative important pathway, formed by an overtone of mode 16, a pure porphyrin in-plane motion, has weak coupling and a good frequency match, resulting in a Fermi resonance parameter of 0.054. No important energy transfer pathways were found for the excited γ_7 mode (8+2, with the largest $r_{S\alpha\beta}$ value of 0.010, is shown in Fig. 4). For the energy transfer from ν_7 to γ_7 overtone and from the overtone of γ_7 to ν_7, the Fermi resonance parameters (0.091 and 0.086, respectively) suggest effective energy exchange between the two modes. However, this channel is not as effective in defining the dominant energy transfer pathway as in FeP due to a relatively bad frequency match. No direct energy transfer was found between the ν_4 and ν_7 modes. All important energy transfer pathways are found to have large geometrical overlap with the system mode (as shown in the supplemental material[46]). Overall, no significant difference was observed in the time scale or pathway for energy transfer upon the change of the central metal from iron to nickel.

Upon breaking the D_{4h} symmetry, the true global minimum was optimized for NiP and found to have lower D_{2d} symmetry. The D_{2d} symmetry NiP was found to be distorted from the planar structure as for the case of the Ni-heme and NiOEP (see Fig. 1). For the nonplanar structure, the ν_4, ν_7, and γ_7 modes of NiP (D_{2d}) were found to have similar frequencies and VER time scales as those observed for the planar NiP (D_{4h}) (see Table I). However, fewer important energy transfer pathways were identified for the excited ν_4 and ν_7 modes (details not shown), indicating the VER pathways were "tuned" by the structural change (see below for detailed discussion).

B. VER of Ni-heme modes

The optimized porphine core of Ni-heme is distorted from the planar structure, similar to the heme in Cyt c (see Fig. 1). The ν_4 mode of the optimized structure was found to be split and the frequency difference between the two modes, modes 147 and 148, is 1.2 cm^{-1}. The fitted VER time constants for the two modes are almost the same, ~1.1 ps (see Table I) and is the same as observed in Fe-heme in our previous study.[34] The calculated mode 74 was assigned as the ν_7 mode. When treated as the system mode, the VER time constant was found to be 2.5 ± 0.1 ps (see Table I), similar to that observed in Fe-heme (2.1 ± 0.1 ps).[34] The time evolution of the excited density matrix element for the ν_4 and ν_7 modes is shown in Fig. 3 (middle).

The third order Fermi resonance parameters of the important VER pathways from the excited ν_4 and ν_7 modes are shown in Fig. 5. Relative to Fe-heme,[34] more important energy transfer pathways are identified for the Ni-heme.

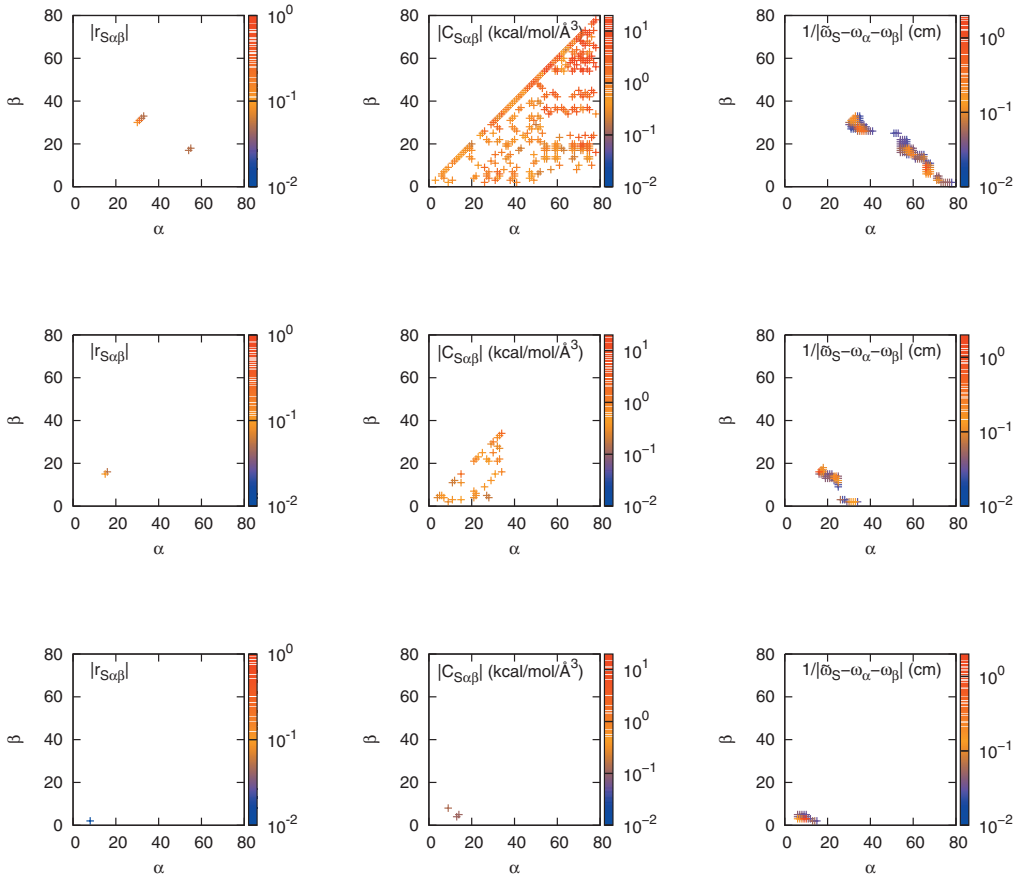

FIG. 4. (Color) The calculated third order Fermi resonance parameter $r_{S\alpha\beta}$ of the important energy transfer pathways, as well as the important coupling constants $C_{S\alpha\beta}$ and the frequency resonance parameter $1/|\tilde{\omega}_S-\omega_\alpha-\omega_\beta|$ for NiP (D_{4h}) modes, from top to bottom, ν_4, ν_7, and γ_7. The x and y axes are the indices of the bath modes.

For each mode accepting energy from the excited ν_4 or ν_7 mode, the norm contributions from the porphine core and from the side chains (defined as $\Sigma(v_{ix}^2+v_{iy}^2+v_{iz}^2)$ with $\mathbf{v}$ being the normal vector and the sum running over all porphine core or side chain atoms, respectively) were calculated. The side chain contribution was further divided into two parts: The contribution from the two isopropionate groups and from the remaining six side chains (as a whole). The results are summarized in the supplemental material.[46] The results for the "dominant" bath modes (with $\geq$0.50 contribution to the norm) or "localized" modes (with $\geq$0.80 contribution) are summarized in Table II.

Most important VER pathways are common for the two split ν_4 modes. For both modes, ~60% of the important pathway modes are dominated by the porphine core motion. While ~40% of the modes are dominated by side chain motion, there are nine modes (14.1% of total) for mode 148 and 7 modes (11.7%) for mode 147 that are dominated by the motion of the two isopropionate groups. These modes are involved in eight important VER pathways from excited mode 148 and five pathways from excited mode 147. Of those with mechanisms of relaxation dominated by other side chains, seven modes involved for excited mode 148 and eight modes involved for excited mode 147 can be found in seven important VER pathways for mode 148 and ten pathways for mode 147. Isopropionate side chain modes and six other side chain modes play a similar role in the VER processes from the excited ν_4 modes. For both excited ν_4 modes, ~20% of the energy accepting modes are localized in the porphine core atoms. There are ten modes localized in the side chains including seven (modes 14, 72, 96, 97, 135, 136, and 138) localized in the two isopropionate side chains for mode 148 and five (modes 14, 72, 135, 136 and 138) for mode 147. In addition, there are four energy accepting modes (modes 122, 132, 133, and 134) for the excited mode 148 and one (mode 132) for the excited mode 147 that, which are localized porphine core in-plane motions. Similar results were obtained from our analysis of VER in the Fe-heme.[34]

Distinct from the mechanism of ν_4 mode relaxation in NiP (D_{4h}), Fe-heme and other Fe porphyrin models, the ν_7 mode in the nonplanar Ni-heme is involved in the important VER pathways from the excited ν_4 modes, including one pathway formed by the ν_7 mode and mode 78 with large third order Fermi resonance parameters (0.727 for mode 148 and 2.275 for mode 147), indicating the possibility of effective energy exchange between the ν_4 and ν_7 modes in Ni-heme.

For the excited ν_7 mode of Ni-heme, there are 23 modes that are involved in the important VER pathways. Similar to Fe-heme,[34] more side chain dominated motions (60.9% of total) are involved as energy accepting modes compared to the excited ν_4 modes. For the 23 energy accepting bath modes, three (modes 45, 47, and 73) are localized in the

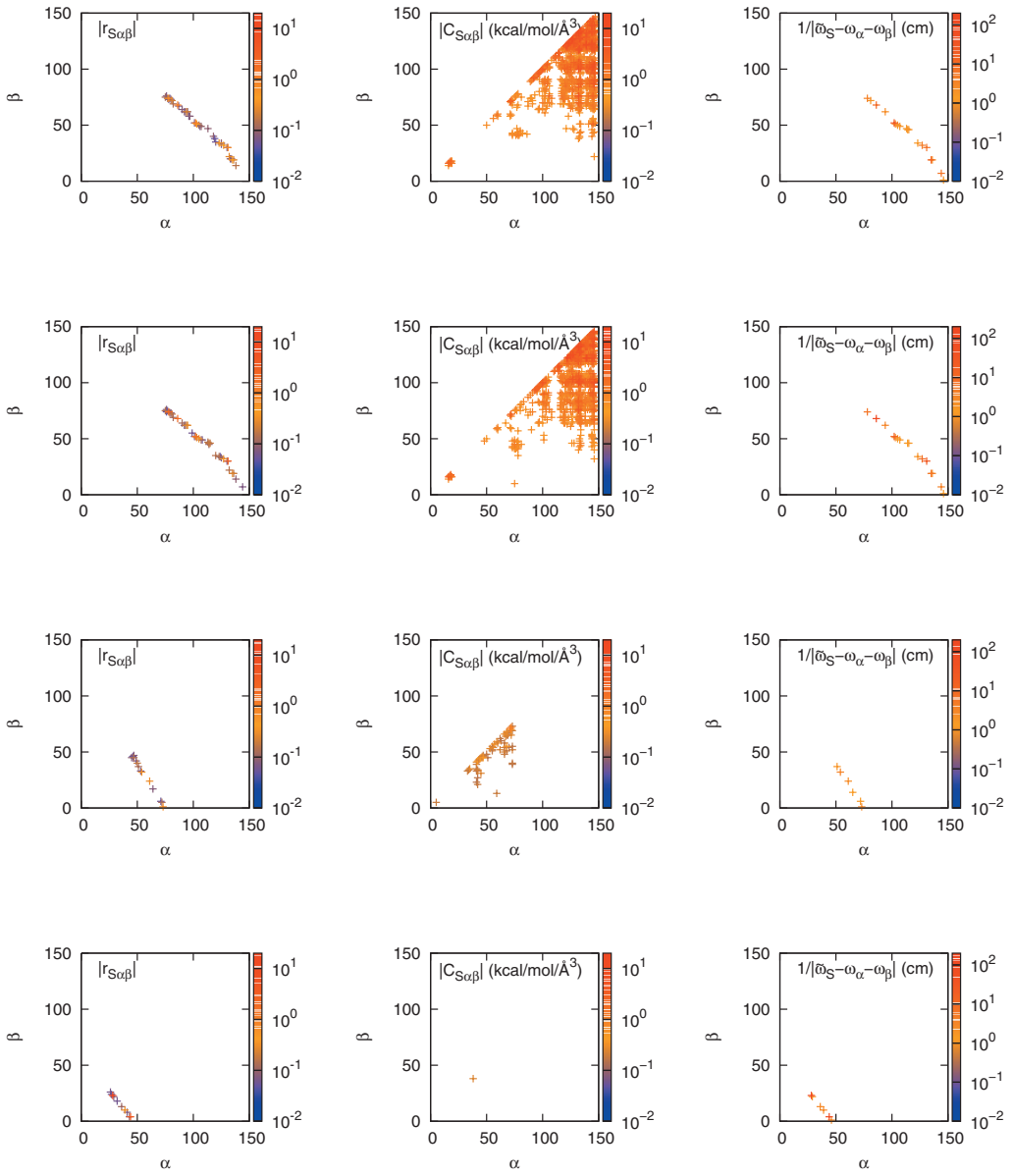

FIG. 5. (Color) The calculated third order Fermi resonance parameter $r_{S\alpha\beta}$ of the important energy transfer pathways, as well as the important coupling constants $C_{S\alpha\beta}$ and the frequency resonance parameter $1/|\tilde{\omega}_S-\omega_\alpha-\omega_\beta|$ for Ni-heme modes, from top to bottom, ν_4 (mode 148), ν_4 (mode 147), ν_7, and γ_7. The x and y axes are the indices of the bath modes.

porphine core and six are localized in the side chains, of which three (modes 5, 71, and 72) are localized in the isopropionate groups and two (modes 1 and 24) others are dominated by the isopropionate group motion. Of the 14 side chain dominant bath modes, seven are dominated by the isopropionate groups and four by the remaining six side chains.

Modes predominately localized in the isopropionate groups are involved in five important VER pathways. Pathways involving isopropionate groups are found to have larger $r_{S\alpha\beta}$ than pathways involving the six other side chain dominant pathways. However, the difference in Ni-heme is not as significant as in Fe-heme.

Similar to NiP (D_{4h}) and Fe porphyrins, the overtone of the γ_7 mode (mode 47) in Ni-heme is found to form an important VER pathway from the excited ν_7 mode. However, the third order Fermi resonance parameter of this pathway (0.079) is small relative to other pathways due to the smaller

TABLE II. Summary of the number of modes involved in the energy transfer pathways from the excited ν_4 and ν_7 modes of the Ni-heme as derived from B3LYP/6-31G(d) calculations.

	Number of bath modes		
Moiety	ν_4 mode (mode 147)	ν_4 mode (mode 148)	ν_7 mode
Total	64	60	23
Porphyrin core ≥0.5	38 (59.4%)	37 (61.7%)	9 (39.1%)
All side chains ≥0.5	26 (40.6%)	23 (38.3%)	14 (60.9%)
Isopropionates ≥0.5	9 (14.1%)	7 (11.7%)	7 (30.4%)
Other side chains ≥0.5	7 (10.9%)	8 (13.3%)	4 (17.4%)
Porphyrin core ≥0.8	14 (21.9%)	12 (20.0%)	3 (13.0%)
All side chains ≥0.8	10 (15.6%)	10 (16.7%)	6 (26.1%)
Isopropionates ≥0.8	7 (10.9%)	5 (8.3%)	3 (13.0%)
Other side chains ≥0.8	2 (3.1%)	3 (5.0%)	0 (0.0%)

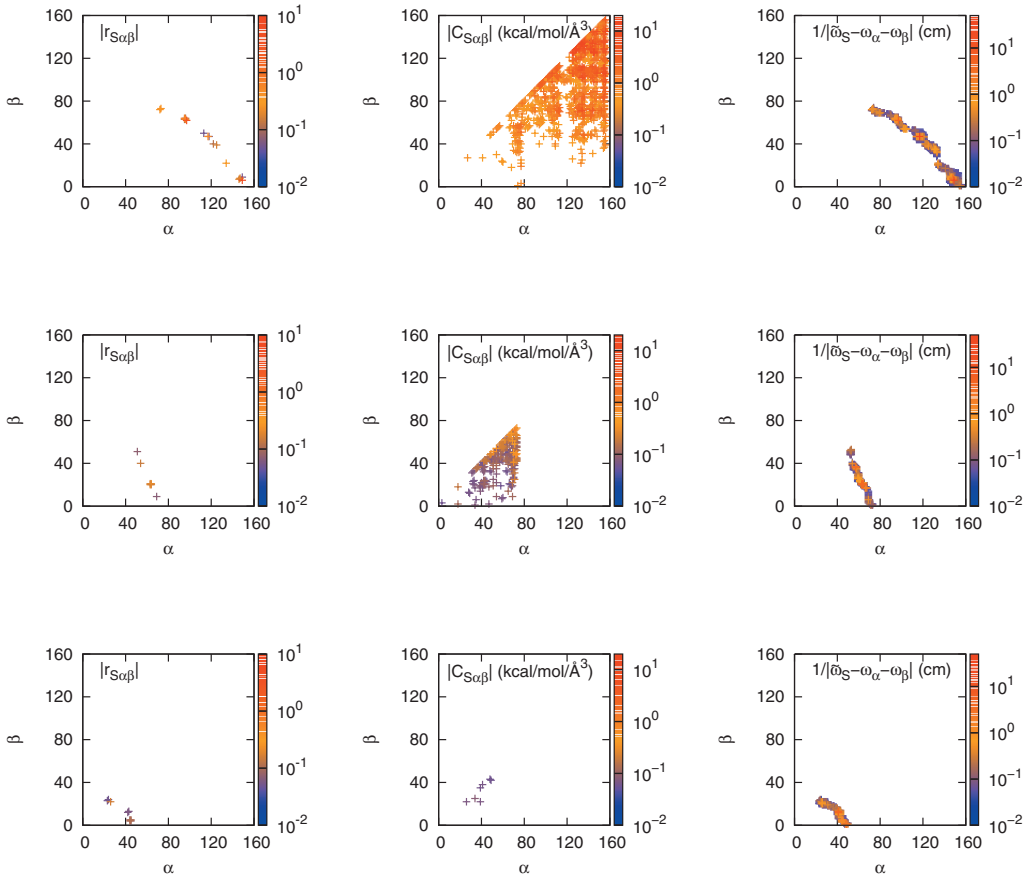

FIG. 6. (Color) The calculated third order Fermi resonance parameter $r_{S\alpha\beta}$ of the important energy transfer pathways, as well as the important coupling constants $C_{S\alpha\beta}$ and the frequency resonance parameter $1/|\tilde{\omega}_S-\omega_\alpha-\omega_\beta|$ for NiOEP modes, from top to bottom, ν_4, ν_7, and γ_7. The x and y axes are the indices of the bath modes.

coupling constant. The third order Fermi resonance parameter for the reverse energy transfer, from the overtone of γ_7 to ν_7, was found to be 0.032, smaller than pathways from the excited γ_7 mode to its lower frequency bath modes (see Fig. 5), indicating a diminished importance of this pathway in energy exchange between the ν_7 mode and the γ_7 mode in Ni-heme relative to Fe-heme.

For the distorted Ni-heme, the isopropionate groups are involved in important energy relaxation channels from the excited ν_4 and ν_7 modes. However, the role is less dominant than observed for the Fe-heme. More porphine core dominated motions are involved for the Ni-heme than in Fe-heme. Distinct from NiP (D_{4h}) and iron porphyrin models, the energy transfer between the ν_4 mode and the ν_7 mode is predicted to be significant in Ni-heme, but the energy exchange between the ν_7 mode and the γ_7 mode, the important energy relaxation channel in Fe-heme, is predicted to be less important in Ni-heme.

C. VER of NiOEP modes

Three crystal structures, two triclinic and one tetragonal, having different orientations of the eight ethyl side chains, have been reported for NiOEP.[47–49] The porphine core is ruffled in the tetragonal NiOEP and planar in the triclinic form. The ruffled configuration is closer to the NiOEP structure in solution[50] and was studied in this work. For the optimized NiOEP, the two ethyl groups on a given pyrrole ring have the same orientation (up or down relative to the porphyrin plane). The ethyl groups on adjacent pyrrole have the opposite orientation (see Fig. 2). As shown in Fig. 1, NiOEP has porphyrin core distortion similar to that observed in the Ni-heme. In addition, the NiOEP has a S_4 symmetry axis through the Ni atom and perpendicular to the porphyrin plane.

The calculated normal modes 157, 74, and 51 were assigned as the ν_4, ν_7, and γ_7 modes, respectively. The VER time constants for the excited ν_4 and ν_7 modes were found to be 1.1 ± 0.0 and 7.0 ± 0.4 ps by single exponential fit (see Table I), faster than the experimentally derived time scale for NiOEP in solution.[30] The time evolution of the excited density matrix elements is shown in Fig. 3 (bottom panel). The calculated third order Fermi resonance parameter $r_{S\alpha\beta}$ for each important VER pathway from the excited system mode, as well as the important coupling constants $C_{S\alpha\beta}$ and the frequency resonance parameter $1/|\tilde{\omega}_S-\omega_\alpha-\omega_\beta|$, are shown in Fig. 6.

For the excited ν_4 mode, about half (42.3%) of the energy accepting modes forming important VER pathways are dominated by porphine core motion, three of which (modes 95, 96, and 97) are localized in the porphine core (see Table III). For those modes dominated by the side chain motions, 11 are found to be localized in the side chains, 42.3% of the 26 bath modes involved in important VER pathways. In addition, 12 out of 26 bath modes are shared by the porphine

TABLE III. Summary of the number of modes involved in the energy transfer pathways from the excited ν_4 and ν_7 modes of the NiOEP as derived from B3LYP/6-31G(d) calculations.

Moiety	Number of bath modes	
	ν_4 mode	ν_7 mode
Total	26	9
Porphyrin core ≥0.5	11 (42.3%)	5 (55.6%)
All side chains ≥0.5	15 (57.7%)	4 (44.4%)
Porphyrin core ≥0.8	3 (11.5%)	1 (11.1%)
All side chains ≥0.8	11 (42.3%)	1 (11.1%)

core and side chains. Although the NiOEP shows similar distortion of the porphine core as observed in Ni-heme, the ν_7 mode is not predicted to be involved in these pathways in NiOEP.

For the excited ν_7 mode, more than half of the energy accepting bath modes, five of nine, are dominated by porphine core motions. (Note that only 29 out of 85 atoms belong to the porphine core.) There is only one essential bath mode (mode 51) localized in the porphine core and one (mode 9) localized in the side chains. The other seven modes are shared by the porphyrin core and the side chains. Mode 51 was found to be the porphine methine wagging motion associated with Ni out-of-plane motion, identified as the γ_7 mode. The γ_7 overtone is strongly coupled to the ν_7 mode in NiOEP ($C_{S\alpha\beta}$=0.584 kcal/mol Å^3), but the third order Fermi resonance parameter $r_{S\alpha\beta}$ (0.073) is smaller than observed for other pathways (see Fig. 6). This result is similar to the nonplanar Ni-heme (see above). Interestingly, the *reverse* energy transfer, from the overtone of γ_7 to ν_7, has a rather large $r_{S\alpha\beta}$ (0.416), similar to our previous predictions for planar Fe porphyrin models.[33,34]

The ν_4 and ν_7 modes are porphine core breathing motions and core dominant motions are strongly involved in the important VER pathways for their relaxation in NiOEP. For the excited ν_4 mode, 10 out of 17 important VER pathways involve core dominant motions, including three mixed core/side chain pathways. For the excited ν_7 mode, six out of seven important VER pathways involve core dominant motions with four being a mixture of side chain and core dominant motions. At the same time, the side chain dominant motions are also involved in VER pathways for the excited ν_4 and ν_7 modes. Ten pathways for the ν_4 mode and five pathways for the ν_7 mode involve side chain dominant motions. This result is similar to our predictions for Ni-heme, in which 23 of 41 and 22 of 38, for the ν_4 modes, and 9 of 14, for the ν_7 mode, involve side chain dominant motions, and 34 of 41 and 34 of 38, for the ν_4 modes, and 9 of 14, for the ν_7 mode, involve core dominant motions. By these pathways, the localized excitation energy (for example, in the ν_4 and ν_7 modes) can efficiently transfer to all atoms forming the moiety including the side chain atoms, assisting energy dissipation from the heme to the environment.

D. Planar and nonplanar porphyrins

Relative to the planar iron porphyrins, different VER features have been observed for the nonplanar nickel porphyrins. One such feature is the predicted direct energy transfer from the excited ν_4 mode to the ν_7 mode. In Ni-heme, the ν_7 mode was predicted to combine with modes 76, 77, 78, or 79 to form important VER pathways from the excited ν_4 mode. No similar pathway was predicted for the planar Fe-heme.

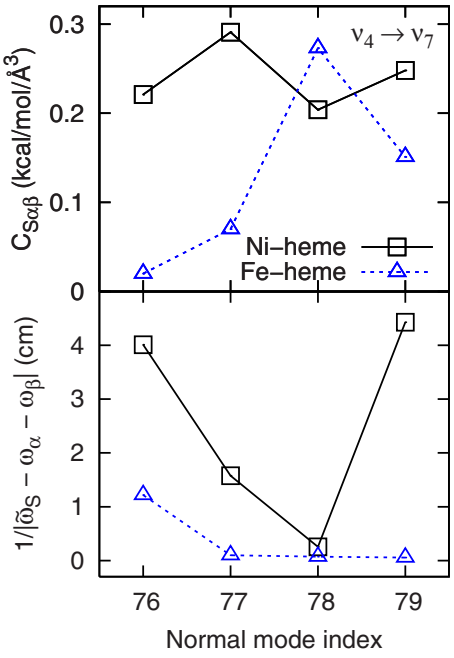

FIG. 7. (Color online) Comparison of the calculated third order coupling constants $C_{S\alpha\beta}$ and the frequency resonance parameters $1/|\tilde{\omega}_S-\omega_\alpha-\omega_\beta|$ of several VER pathways involving the ν_7 mode for the excited ν_4 mode of Ni-heme (square) and Fe-heme (triangle). The *x*-axis is the bath mode index that "dresses" the ν_7 mode in the VER pathway.

In this work, important VER pathways were identified using the third order Fermi resonance parameters, which are proportional to the third order coupling constant $C_{S\alpha\beta}$ and the frequency resonance parameter $1/|\tilde{\omega}_S-\omega_\alpha-\omega_\beta|$, as indicated by Eq. (8). In Fig. 7, the coupling constant $C_{S\alpha\beta}$ and frequency resonance parameter $1/|\tilde{\omega}_S-\omega_\alpha-\omega_\beta|$ are plotted versus the index of the bath mode "dressing" the ν_7 mode to form important VER pathways in Ni-heme as well as the corresponding pathways in Fe-heme. (The corresponding normal modes of Fe-heme were identified by checking the dot product of the normal mode eigenvectors of the two molecules.) The $C_{S\alpha\beta}$ values of all four pathways in Ni-heme fall in the range of 0.2–0.3 kcal/mol Å^3. In Fe-heme, only one pathway, formed by mode 78 and the ν_7 mode, has $C_{S\alpha\beta}$ in the same range. For the frequency resonance parameters, the ν_7+mode 76 combination in Fe-heme has the strongest resonance with the excited ν_4 mode. However, it is about four times smaller than the corresponding resonance in Ni-heme. Other pathways of Fe-heme have even smaller frequency resonance parameters and all are predicted to be smaller than those computed for Ni-heme. As a result, due to the weak coupling and/or bad frequency match, the ν_7 mode is not predicted to be essential to the VER of the ν_4 mode in Fe-heme.

An additional difference between the planar porphyrin models and nonplanar models is predicted to be the energy transfer from the excited ν_7 mode to the overtone of the γ_7 mode. This was found to be the dominant pathway for relax-

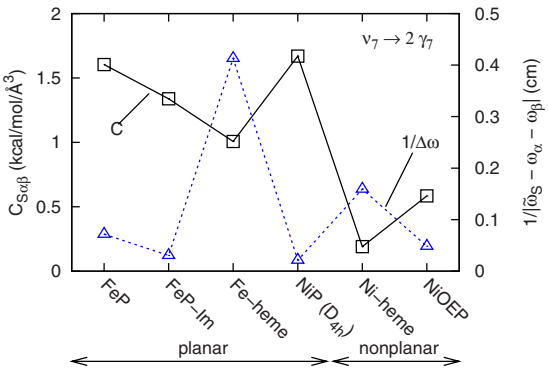

FIG. 8. (Color online) The calculated third order coupling constants $C_{S\alpha\beta}$ (square) and the frequency resonance parameters $1/|\tilde{\omega}_S - \omega_\alpha - \omega_\beta|$ (triangle) of the ν_7 to γ_7 overtone relaxation pathway of the planar and nonplanar porphyrin models.

ation of the excited ν_7 mode in the planar porphyrins, but is found to be absent in the nonplanar Ni-heme and NiOEP. The third order coupling constant $C_{S\alpha\beta}$ and the frequency resonance parameter $1/|\tilde{\omega}_S - \omega_\alpha - \omega_\beta|$ for the pathway involving the overtone of γ_7 are plotted in Fig. 8 for each porphyrin model. This combination is predicted to have a small frequency resonance parameter $1/|\tilde{\omega}_S - \omega_\alpha - \omega_\beta|$ in all the porphyrin models. Fe-heme has a relatively larger value. For the coupling constants, all planar porphyrins have values greater than 1 kcal/mol Å^3, while values for nonplanar porphyrins are much smaller, leading to the small Fermi resonance parameters predicted for Ni-heme and NiOEP.

It is clear from the above discussion that both the normal mode frequencies and the coupling constants change upon distortion of the porphyrin from a planar structure. Changes in structure leading to modulation of coupling constants play an essential role in "tuning" the important VER pathways for energy relaxation from the excited ν_4 and ν_7 modes.

IV. SUMMARY AND CONCLUSIONS

The mode-specific VER of the ν_4 and ν_7 modes of three nickel porphyrin models, the NiP, Ni-heme, and NiOEP were studied using the time-dependent perturbation theory at the B3LYP/6-31G(d) level. NiP (D_{4h}) was found to be planar. The porphine cores of Ni-heme and NiOEP were found to be distorted, similar to the heme in the crystal structure of Cyt c.[13] The ν_4 and ν_7 modes were assigned for each molecule and the VER time scales and pathways were identified independently.

The core size of NiP (D_{4h}) was found to be 1.957 Å, smaller than that of FeP (1.988 Å) (Ref. 34) due to the smaller size of Ni relative to Fe. However, the derived time constants of ν_4 and ν_7 modes of NiP (D_{4h}) are similar to those of FeP and the important energy transfer pathways are similar to those predicted for FeP. We conclude that the mechanism and time scale of VER of the ν_4 and ν_7 modes are not affected by the change of the porphyrin central metal.

The nickel porphine core structure was displaced from a planar geometry by adding the side chains. For Ni-heme the predicted VER time constants of the excited ν_4 modes and ν_7 mode, ~1.1 and ~2.5 ps, respectively, are similar to the predictions for the planar Fe-heme[34] and previous experiments on MbCO.[24] However, the energy transfer pathways have distinct characteristics. When the ν_4 mode was treated as the excited system mode, the ν_7 mode was found to play an essential role in its energy relaxation pathways. For the excited ν_7 mode, the effective energy exchange pathway between the ν_7 mode and the overtone of the γ_7 mode, observed in planar iron porphyrin models, was predicted to be insignificant in the nonplanar Ni-heme. The heme isopropionate groups were found to be involved in the VER processes of the excited ν_4 and ν_7 modes in Ni-heme, but not more important than the other side chains.

The NiOEP has a ruffled porphine core structure similar to that observed for Ni-heme. With eight ethyl side chains, NiOEP has higher symmetry than Ni-heme. The coupling between the ν_7 mode and the overtone of the γ_7 mode is weak and plays a less important role than other pathways, indicating that this coupling is sensitive to the porphine core distortion. A similar prediction is made for the nonplanar Ni-heme. The energy transfer between the ν_4 and ν_7 mode can be affected by many factors, such as the frequencies of the two modes. We predicted that direct energy transfer between the ν_4 and ν_7 modes is insignificant in NiOEP.

The ν_4 and ν_7 modes are porphine core in-plane motions. However, for both Ni-heme and NiOEP, the side chain dominant modes are strongly involved in the important energy transfer pathways of the excited ν_4 and ν_7 modes. We conjecture that this coupling is an essential component of energy dissipation from the heme to the surrounding environment. Compared to planar porphyrin models, vibrational resonance and coupling constants between the system and bath modes are "tuned" by the distortion of the porphine core structure, leading to essential differences in the time scales and pathways for VER in these porphyrin systems.

ACKNOWLEDGMENTS

We are grateful for the generous support of this research by the National Science Foundation (Grant Nos. CHE-0316551 and CHE-0750309) and Boston University's Center for Computational Science.

[1] M. C. Asplund, M. T. Zanni, and R. M. Hochstrasser, Proc. Natl. Acad. Sci. U.S.A. **97**, 8219 (2000).
[2] Y. Kholodenko, M. Volk, E. Gooding, and R. M. Hochstrasser, Chem. Phys. **259**, 71 (2000).
[3] P. Li, J. T. Sage, and P. M. Champion, J. Chem. Phys. **97**, 3214 (1992).
[4] J. W. Petrich, C. Poyart, and J. L. Martin, Biochemistry **27**, 4049 (1988).
[5] M. Lim, T. A. Jackson, and P. A. Anfinrud, J. Phys. Chem. **100**, 12043 (1996).
[6] W. Wang, X. Ye, A. A. Demidov, F. Rosca, T. Sjodin, W. Cao, M. Sheeran, and P. M. Champion, J. Phys. Chem. B **104**, 10789 (2000).
[7] M. Negrerie, S. Cianetti, M. H. Vos, J.-L. Martin, and S. G. Kruglik, J. Phys. Chem. B **110**, 12766 (2006).
[8] D. E. Sagnella and J. E. Straub, J. Phys. Chem. B **105**, 7057 (2001).
[9] L. Bu and J. E. Straub, J. Phys. Chem. B **107**, 10634 (2003).
[10] L. Bu and J. E. Straub, J. Phys. Chem. B **107**, 12339 (2003).
[11] J. Kuriyan, S. Wilz, M. Karplus, and G. A. Petsko, J. Mol. Biol. **192**, 133 (1986).
[12] G. S. Kachalova, A. N. Popov, and H. D. Bartunik, Science **284**, 473 (1999).
[13] G. W. Bushnell, G. V. Louie, and G. D. Brayer, J. Mol. Biol. **214**, 585 (1990).
[14] Y. Zhang and J. E. Straub, J. Phys. Chem. B **113**, 825 (2009).

[15] Y. Zhang, H. Fujisaki, and J. E. Straub, J. Phys. Chem. B **111**, 3243 (2007).
[16] F. Rosca, A. T. N. Kumar, X. Ye, T. Sjodin, A. A. Demidov, and P. M. Champion, J. Phys. Chem. A **104**, 4280 (2000).
[17] F. Rosca, A. T. N. Kumar, D. Ionascu, T. Sjodin, A. A. Demidov, and P. M. Champion, J. Chem. Phys. **114**, 10884 (2001).
[18] F. Rosca, A. T. N. Kumar, D. Ionascu, X. Ye, A. A. Demidov, T. Sjodin, D. Wharton, D. Barrick, S. G. Sligar, T. Yonetani, and P. M. Champion, J. Phys. Chem. A **106**, 3540 (2002).
[19] P. M. Champion, F. Rosca, D. Ionascu, W. Cao, and X. Ye, Faraday Discuss. **127**, 123 (2004).
[20] F. Gruia, X. Ye, D. Ionascu, M. Kubo, and P. M. Champion, Biophys. J. **93**, 4404 (2007).
[21] A. M. Nagy, V. Raicu, and R. J. D. Miller, Biochim. Biophys. Acta **1749**, 148 (2005).
[22] M. R. Armstrong, J. P. Ogilvie, M. L. Cowan, A. M. Nagy, and R. J. D. Miller, Proc. Natl. Acad. Sci. U.S.A. **100**, 4990 (2003).
[23] Y. Mizutani and T. Kitagawa, Science **278**, 443 (1997).
[24] Y. Mizutani and T. Kitagawa, Chem. Rec. **1**, 258 (2001).
[25] S. G. Kruglik, P. Mojzes, Y. Mizutani, T. Kitagawa, and P.-Y. Turpin, J. Phys. Chem. B **105**, 5018 (2001).
[26] T. Kitagawa, N. Haruta, and Y. Mizutani, Biopolymers **67**, 207 (2002).
[27] J. Rodriguez and D. Holten, J. Chem. Phys. **91**, 3525 (1989).
[28] J. Rodriguez, C. Kirmaier, and D. Holten, J. Chem. Phys. **94**, 6020 (1991).
[29] Y. Mizutani and T. Kitagawa, Bull. Chem. Soc. Jpn. **75**, 623 (2002).
[30] Y. Mizutani, Y. Uesugi, and T. Kitagawa, J. Chem. Phys. **111**, 8950 (1999).
[31] Y. Mizutani and T. Kitagawa, J. Mol. Liq. **90**, 233 (2001).
[32] Y. Mizutani and T. Kitagawa, Bull. Chem. Soc. Jpn. **75**, 965 (2002).
[33] Y. Zhang, H. Fujisaki, and J. E. Straub, J. Chem. Phys. **130**, 025102 (2009).
[34] Y. Zhang and J. E. Straub, J. Chem. Phys. **130**, 095102 (2009).
[35] X. Ye, A. Demidov, F. Rosca, W. Wang, A. Kumar, D. Ionascu, L. Zhu, D. Barrick, D. Wharton, and P. M. Champion, J. Phys. Chem. A **107**, 8156 (2003).
[36] Y. Gao, M. Koyama, S. F. El-Mashtoly, T. Hayashi, K. Harada, Y. Mizutani, and T. Kitagawa, Chem. Phys. Lett. **429**, 239 (2006).
[37] M. Koyama, S. Neya, and Y. Mizutani, Chem. Phys. Lett. **430**, 404 (2006).
[38] H. Fujisaki, Y. Zhang, and J. E. Straub, J. Chem. Phys. **124**, 144910 (2006).
[39] N. Matsuzawa, M. Ata, and D. A. Dixon, J. Phys. Chem. **99**, 7698 (1995).
[40] H. Fujisaki, L. Bu, and J. E. Straub, Adv. Chem. Phys. **130**, 179 (2005).
[41] M. J. Frisch, G. W. Trucks, H. B. Schlegel, *et al.*, GAUSSIAN 03, Revision C.02, Gaussian, Inc., Wallingford, CT, 2004.
[42] K. Moritsugu, O. Miyashita, and A. Kidera, J. Phys. Chem. B **107**, 3309 (2003).
[43] J. L. Hoard, Science **174**, 1295 (1971).
[44] W. Jentzen, I. Tyrowska-Tyrk, W. R. Scheidt, and J. A. Shelnutt, Inorg. Chem. **35**, 3559 (1996).
[45] P. M. Kozlowski, T. S. Rush III, A. A. Jarzecki, M. Z. Zgierski, B. Chase, C. Piffat, B.-H. Ye, X.-Y. Li, P. Pulay, and T. G. Spiro, J. Phys. Chem. A **103**, 1357 (1999).
[46] See EPAPS Document No. E-JCPSA6-130-017923 for the supplementary material. For more information on EPAPS, see http://www.aip.org/pubservs/epaps.html.
[47] E. F. Meyer, Jr., Acta Crystallogr., Sect. B: Struct. Crystallogr. Cryst. Chem. **28**, 2162 (1972).
[48] D. L. Cullen and E. F. Meyer, Jr., J. Am. Chem. Soc. **96**, 2095 (1974).
[49] T. D. Brennan, W. R. Scheidt, and J. A. Shelnutt, J. Am. Chem. Soc. **110**, 3919 (1988).
[50] R. S. Czernuszewicz, X. Li, and T. G. Spiro, J. Am. Chem. Soc. **111**, 7024 (1989).